Electromagnetic Interference Shielding Behavior of Polyaniline/Graphite Composites Prepared by *In Situ* Emulsion Pathway

Parveen Saini,[1] Veena Choudhary,[2] K. N. Sood,[3] S. K. Dhawan[1]

[1]*Polymeric and Soft Materials Section, National Physical Laboratory, New Delhi 110012, India*
[2]*Centre for Polymer Science and Engineering, Indian Institute of Technology, New Delhi 110016, India*
[3]*Electron Microscopy Section, National Physical Laboratory, New Delhi 110012, India*

Received 19 May 2008; accepted 12 November 2008
DOI 10.1002/app.30183
Published online 7 May 2009 in Wiley InterScience (www.interscience.wiley.com).

ABSTRACT: Polyaniline–graphite composites were prepared via in situ emulsion pathway, using different weight ratios of aniline to graphite. These composites were characterized for thermal, electrical, and spectral attributes. The thermal stability (~ 230°C) and electrical conductivity (67.9 S/cm) were improved significantly as compared with polyaniline doped with conventional inorganic dopants such as HCl (140°C and 10 S/cm). Scanning electron micrographs indicated a systematic change in morphology from globular to flaky with increasing amounts of graphite. The relative shifting of UV–visible bands indicates that some interactions exist between doped polyaniline and graphite. Absorption-dominated total electromagnetic interference shielding effectiveness of the order of −33.6 dB suggests that these materials can be used as futuristic microwave shielding materials. The good electrical conductivity and thermal stability make them ideal candidates for preparing conducting composites by melt blending with conventional thermoplastics such as polyethylene, polypropylene, and polystyrene, etc. © 2009 Wiley Periodicals, Inc. J Appl Polym Sci 113: 3146–3155, 2009

Key words: polyaniline; graphite; conducting polymers; emulsion polymerization; EMI shielding effectiveness; microwave absorption

INTRODUCTION

The conducting polymers have emerged as an important class of materials with specialized applications such as energy storage,[1,2] sensors,[3–5] anticorrosive materials,[6–8] electromagnetic interference shielding (EMI),[9–11] electrostatic charge dissipation (ESD),[12–14] organic light emitting diodes (OLEDs),[15–18] solar cells,[19,20] and catalysis.[21,22] However, among other conducting polymers, polyaniline has a special status due to its nonredox doping (leading to polaron lattice),[23] good environmental stability, and economic feasibility. In addition to the above properties, it also possesses acceptable electrical conductivity and thermal stability. Despite all these advantages, the main drawback of polyaniline is processing difficulties due to its infusibility and relative insolubility in common organic solvents. The processing issue can be solved by using functionalized anilines[24,25] or by copolymerization.[26–28] Judicial selection of counter-ions can also improve processability.[29,30] However, these improvements in processability often lead to measurable decreases in conductivity. One way to achieve good processability as well as high electrical conductivity and thermal stability is by incorporation of graphite as a conducting filler material. There are several reports on synthesis of composites of polyaniline with conducting materials such as graphite,[31] exfoliated graphite,[32] carbon black,[33] colloidal graphite, and carbon nanotubes.[34,35] However, there are only few brief reports on synthesis and microwave shielding studies of highly conducting polyaniline graphite composites. In this work, polyaniline–graphite composites were prepared by in situ emulsion pathways to achieve the combination of good processability (solution or melt), adequate thermal stability, and high electrical conductivity. These attributes are desirable for achieving efficient and economical microwave absorbers. The composites so synthesized were characterized by the various techniques such as TGA, FTIR, UV–visible spectroscopy, and XRD. Their electrical conductivities were measured by a four-probe technique, and morphologies were observed using scanning electron microscopy (SEM) and transmission electron microscopy (TEM). The EMI shielding effectiveness was measured by Vector network analyzer. The high thermal stability and acceptable electrical conductivity values suggest that these polymers can be melt blended with conventional thermoplastics such as polyethylene (PE), polypropylene (PP), or polystyrene (PS).

Correspondence to: S. K. Dhawan (skdhawan@mail.nplindia.ernet.in).

EXPERIMENTAL DETAILS

Materials

Aniline (Loba Chemie, India) was freshly distilled before use. Dodecyl benzene sulfonic acid (DBSA, Merck, India), graphite powder (Merck, India, fine powder <50 μm, bulk density ~ 280 kg/m^3), ammonium persulfate (APS, Merck, India), isopropyl alcohol (Merck, India), and chloroform (Qualigens, India) were used as received. Aqueous solutions were prepared from double-distilled water with specific resistivity of 10^6 Ω cm.

Polymer preparation

Synthesis of polyaniline

The polyaniline was prepared by free radical chemical oxidative polymerization of aniline via direct route.[36] The DBSA acts as dopant as well as surfactant and the reaction assumes the characteristics of typical emulsion polymerization. In a typical reaction, 0.1 mol of aniline and 0.3 mol DBSA were added to 1.0 L of distilled water. The mixture was homogenized using a high-speed blender (ART MICCRA D8, rotating at 10,800 rpm) for 30 min to form a stable emulsion. The emulsion was transferred to a double-walled glass reactor and cooled to −5.0°C under constant stirring (900 rpm). The polymerization was initiated by dropwise addition of ammonium persulfate (100 mL aqueous solution of 0.1*M* APS) and temperature was maintained at −5.0°C ± 1.0°C throughout the course of reaction (6 h). The polymer was produced directly in the doped state as dark green slurry (latex). At this stage, excess isopropyl alcohol was added to destabilize the emulsion, and stirring was continued for another 2 h. The polymer particles were isolated from destabilized emulsion by filtration. The wet polymer cake was thoroughly dried at 80°C under dynamic vacuum, and the dried lumps were crushed to obtain the powdered polyaniline (GDBS0).

Synthesis of composites

The composites were also prepared by emulsion polymerization. The quantities of aniline and DBSA were kept the same as during synthesis of pure polyaniline (GDBS0), and the calculated (according to intended weight percentage in composite) amount of graphite powder was added to the above mixture. The system was homogenized using a high-speed blender to form stable emulsion. The formed emulsion was then polymerized using ammonium persulfate under the same conditions as for pure polyaniline (GDBS0). Finally, the powdered composites were obtained by latex destabilization, filtration, and drying. The different compositions containing 10, 30, 50, 70, and 90% of graphite (relative to aniline monomer) were prepared for comparison and designated as GDBS10, GDBS30, GDBS50, GDBS70, and GDBS90, respectively. The control graphite samples was also prepared and designated as GDBS100.

Measurements

The conductivities of pressed pellets of 13-mm length, 7-mm width, and 2-mm thickness were measured by four-point probe technique, using Keithley 220 Programmable Current Source and 181 Nanovoltmeter. A Thermogravimetric analyzer (Mettler Toledo TGA/SDTA 851^e) was used to observe the thermal stability of the material under inert atmosphere in the temperature range of 25–700°C. The samples were also studied by UV–visible (Shimadzu UV-1601), infrared (FTIR, NICOLET 5700), and XRD (D8 Advance Bruker AXS X-ray diffractometer) techniques. Morphologies were observed using SEM (Leo 440S, UK) and TEM (Phillips, CM-12). EMI shielding effectiveness (SE) values were measured by placing rectangular pellets (2-mm thick) inside X-band (8.2–12.4 GHz) waveguides, using a Vector Network Analyzer (VNA E8263BAgilent Technologies).

RESULTS AND DISCUSSION

Mechanism of formation of composites

The mechanistic formation of composites is depicted schematically in Figure 1. The difficulty in dispersing hydrophobic graphite particles in the aqueous medium (generally used for the polymerization of aniline) was solved using DBSA as surfactant dopant. The graphite phase [Fig. 1(a)] was added to aqueous aniline-DBSA emulsion [Fig. 1(b)]. The mixture was homogenized further to obtain the uniform dispersion of the graphite phase in the emulsion [Fig. 1(c)]. The polymerization was initiated by dropwise addition of oxidant with proper temperature control. The oxidative polymerization of aniline shows an induction period after which the color of reaction medium turns green. This indicates onset of polymerization. The presence of graphite phase in the reaction mass shows an accelerating effect on the rate of oxidation of aniline. Therefore, the increase in the graphite content leads to the shortening of induction period and faster color production. The theory of heterogeneous catalysis can be used to explain the faster oxidation of aniline in the presence of the graphite phase.[37] The graphite has a flaky morphology with layered structure. The high specific surface area of graphitic sheets provides a large

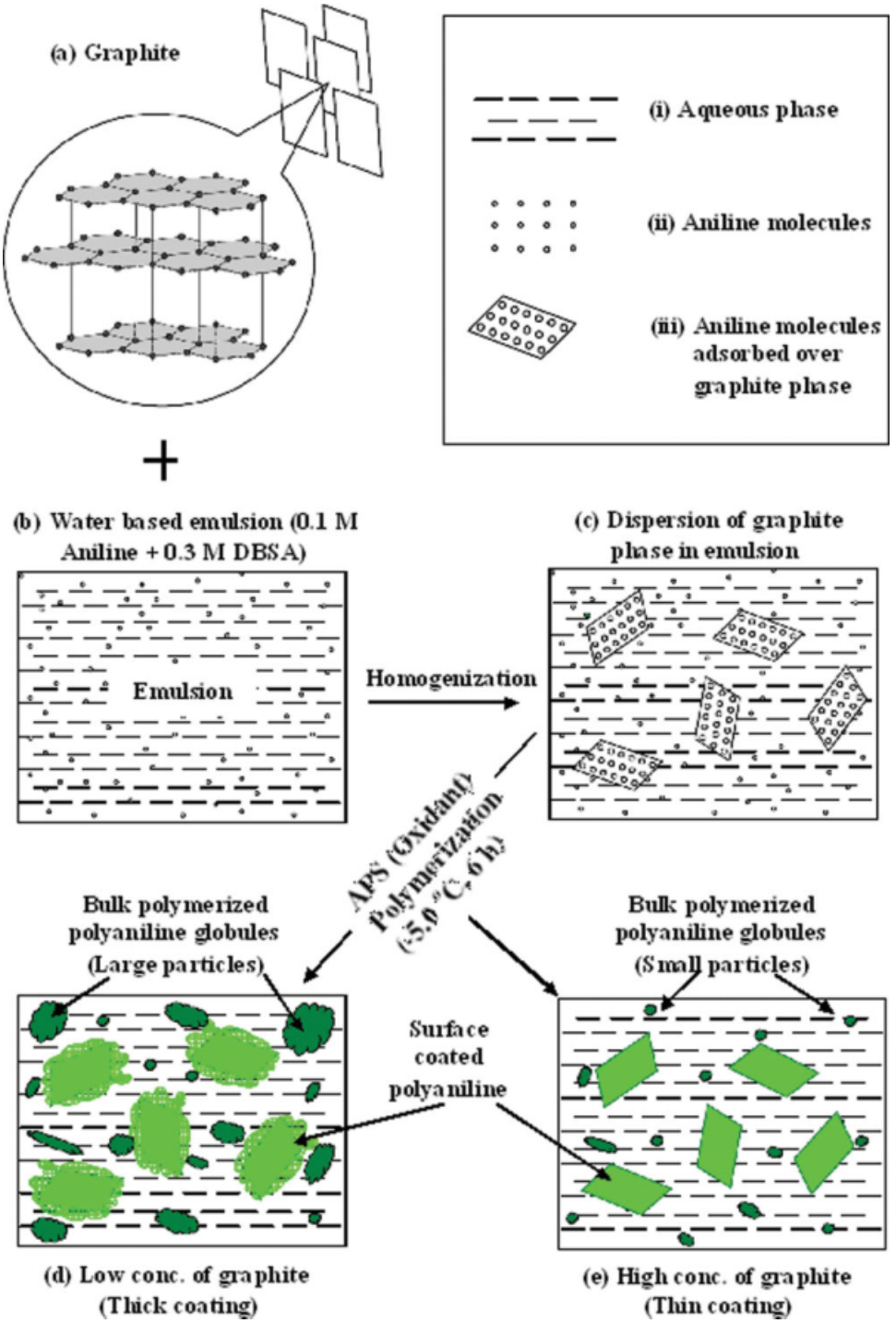

Figure 1 Proposed mechanism for formation of composites. [Color figure can be viewed in the online issue, which is available at www.intersience.wiley.com.]

number of binding sites for adsorption and absorption of aniline monomer. Therefore, like other large surface area materials, graphite should also work like a catalyst by increasing the effective collision frequency of reactants, which leads to faster reaction rates. The oxidation of aniline proceeds via typical redox mechanism, where electrons are abstracted from aniline monomer and are accepted by the oxidant moieties (ammonium peroxydisulfate). The graphite (excellent electrical conductor) phase can mediate the transfer of electrons between the aniline and oxidant. This suggests that a molecule of aniline in contact with graphite can be oxidized even without direct contact with the oxidant molecule, which can transfer the electrons to graphite phase. Therefore, the probability of oxidative polymerization of

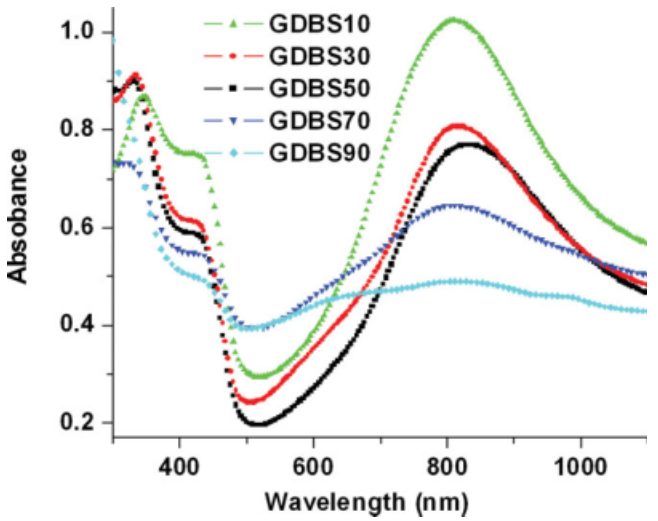

Figure 2 UV–visible spectra of polyaniline–graphite composites. [Color figure can be viewed in the online issue, which is available at www.intersience.wiley.com.]

aniline is much higher on the graphite surface than in solution phase (bulk). The conducting polyaniline chains on the graphite surface also participate in the electron transfer process. In addition, graphite is an excellent conductor of heat, whereas polyaniline has a very low thermal conductivity. Therefore, incorporation of graphite within the polyaniline matrix helps in heat management during polymerization and leads to uniform coating over graphite particles. Two different polymerization situations can be visualized, as shown in Figure 1 and discussed below:

a. At very low concentration of graphite [Fig. 1(d)], the solution/bulk polymerization of aniline dominated over surface polymerization (at graphite aniline interface). Therefore, large agglomerates of polyaniline were formed in the solution phase with irregular and thick coating over graphite layers. The system assumes highly agglomerated globular morphology with polyaniline as the semiconducting matrix and graphite as the conducting filler.
b. However, at very high concentrations of graphite [Fig. 1(e)], the surface polymerization of aniline was the dominant mode. Therefore, minute agglomerates of polyaniline are formed in the bulk phase, and uniform coating of polyaniline was formed over the graphitic layers. The system therefore exhibits layered morphology with graphite as a highly conducting matrix and the semiconducting polyaniline phase as interlayer material.

UV–visible absorption spectra

For UV–visible measurements, a 1.0-mg sample was dissolved in 10 mL of chloroform and subjected to ultrasonication (30 min). Solution was filtered, and about 1.0 mL of the filtrate was taken and further diluted to 10 mL. This solution was then filled in quartz cuvettes and the UV spectrum was recorded.

These spectra are shown in Figure 2, and characteristic bands are presented in Table I. The band around 340 nm is ascribed to the $\pi \rightarrow \pi^*$ transition, whereas bands around 435 nm (polaron$\rightarrow\pi^*$) and 815 nm ($\pi\rightarrow$polaron)[36] are the characteristics of localized polaronic states and indicate that the polymers are present in the doped form. The results revealed that with the increase in graphite content, these bands show systematic shifting. This indicates change in the chain configuration and degree of charge localization. As the graphite fraction increases, the 815-nm band shows a red shift and becomes broad and less prominent. This may be attributed to the increased charge delocalization over the polymeric backbone due to the formation of charge transfer complex between doped polyaniline and the graphite phase. The 435-nm band also shows a red shift with increasing graphite content, further confirming formation of the charge transfer complex. These interactions are due to complexation with benzenoid and quinoid units of polyaniline.[34,38]

TABLE I
Thermal, Electrical, and Structural Attributes of Polyaniline–Graphite Composites

Sample	Conductivity (S/cm)	IDT (°C)	Graphite content (wt %)		Average EMI SE (dB)	UV–visible bands, λ (nm)
			Taken in initial reaction mixture	Calculated from char residue in TGA		
GDBS0	2.1	230	0.0	0.0	−18.4	350, 438, 780
GDBS10	5.0	235	10.0	9.3	−29.2	342, 434, 811
GDBS30	12.5	238	30.0	15.6	−33.6	333, 437, 816
GDBS50	11.8	234	50.0	26.6	−28.4	331, 436, 830
GDBS70	22.7	231	70.0	44.5	−28.2	337, 440, 813
GDBS90	67.9	227	90.0	56.7	−27.4	443, 815
GDBS100	–	700	100.0	100.0	–	–

IDT, initial decomposition temperature, i.e., temperature at which weight loss was first observed in the TG plots.

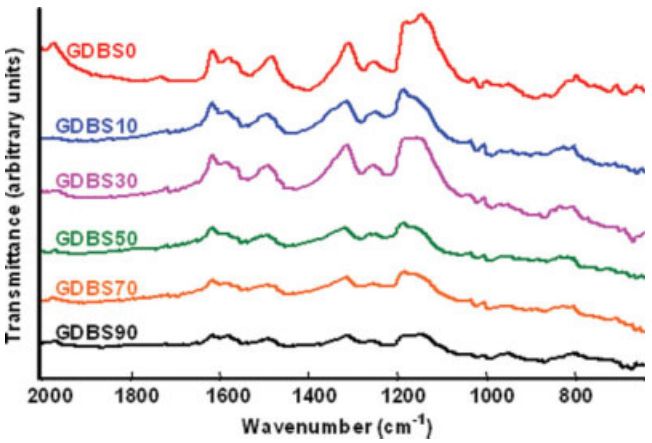

Figure 3 FTIR spectra of polyaniline and polyaniline–graphite composites. [Color figure can be viewed in the online issue, which is available at www.intersience.wiley.com.]

FTIR spectra

Figure 3 shows the FTIR spectra of pure polyaniline and doped composites. The spectra of all composites give the characteristic bands of both benzenoid and quinoid units, which confirms the presence of polyaniline. Also in the region 1650–1400 cm^{-1}, bands due to aromatic ring breathing, N—H deformation and C—N stretching are observed. The 1550 and 1455 cm^{-1} bands are due to nitrogen quinoid (N=Q=N) and benzenoid (N—B—N), respectively, and represent the conducting state of polymer. The bands around 1285 and 1230 cm^{-1} are assigned to the bending vibrations of N—H and asymmetric C—N stretching modes of benzenoid rings, respectively. The absorption band around 1060 cm^{-1} (C—N stretching) is due to the charge delocalization over the polymeric backbone.[36] The 1030 and 865 cm^{-1} bands are due to the stretching vibrations of SO_3^- (of the dopant DBSA) and out of plane C—H bending vibrations, respectively. As the amount of graphite increases, these bands become flatter (Fig. 2). A slight shifting and broadening of characteristic bands was also observed with increasing graphite phase, which indicates existence of interactions between graphite and polyaniline. However, absences of any new vibration bands suggest that interactions are purely physical in nature without any chemical origin.

Morphological characterization

The SEM micrographs [Fig. 4(a–g)] of pure polyaniline and composites clearly show the presence of flakes (having layered morphology) in the case of pure graphite powder (GDBS100) and highly agglomerated globular morphology in doped polyaniline (GDBS0). However, composites show a systematic change in morphology from globular (graphite in polyaniline matrix) to layered (polyaniline in graphite matrix) with the increase in graphite fraction. This may be attributed to the high specific surface area of the graphite layers that provides large numbers of binding sites to polyaniline. Therefore, at low graphite content, polyaniline-coated graphite flakes exist as globular agglomerates. However, at higher graphite concentrations, matrix changeover takes place and therefore composites assume the characteristic layered morphology of graphite. TEM [Fig. 4(h)] of the GDBS50 clearly shows the presence of randomly scattered polydisperse graphite particles in the polyaniline matrix. The TEM picture revealed that the average diameter of the polydisperse graphite particles was in the range of 20–25 nm.

XRD studies

Figure 5 shows the powder XRD pattern of the doped composites. The pattern shows a sharp peak centered on 2θ value of 26°, which corresponds to the graphite (002 planes),[39] and its intensity increases monotonically with increase in the graphite content. Further, this peak shows an initial shift with an increase in graphite content. However, at higher concentrations, it comes back to the original position. This indicates that initially the interactions between graphite and polyaniline increases and then stabilizes, especially at higher content.

The composite also shows characteristic peaks of the doped polyaniline around 20° and 25° that were absent in the XRD spectra of the pure graphite powder (inset Fig. 4). However, these peaks are actually masked by the intense peak of the graphite and appear as a faint shoulder. The average crystallite size of graphite domains in the composites can be estimated from the broadening of the diffraction peaks (002 planes), using Scherrer formula[36]:

$$D = \frac{k\lambda}{\beta \cos\theta}, \quad (1)$$

where D is the average crystallite size, λ is the X-ray wavelength (1.5404 Å), β is the full-width at half-maximum (FWHM), and θ is the diffraction angle. The value of k depends on several factors, including the Miller index of reflection plane and the shape of the crystal, etc. If shape is unknown, k is often assigned a value of 0.89. As determined from eq. (1), the average crystallite size of the GDBS50 was 18 nm, which is in accordance with TEM measurements.

Conductivity

The compressed rectangular pellets were subjected to current–voltage scans, and the resistance of the material was obtained by Ohm's law. The room

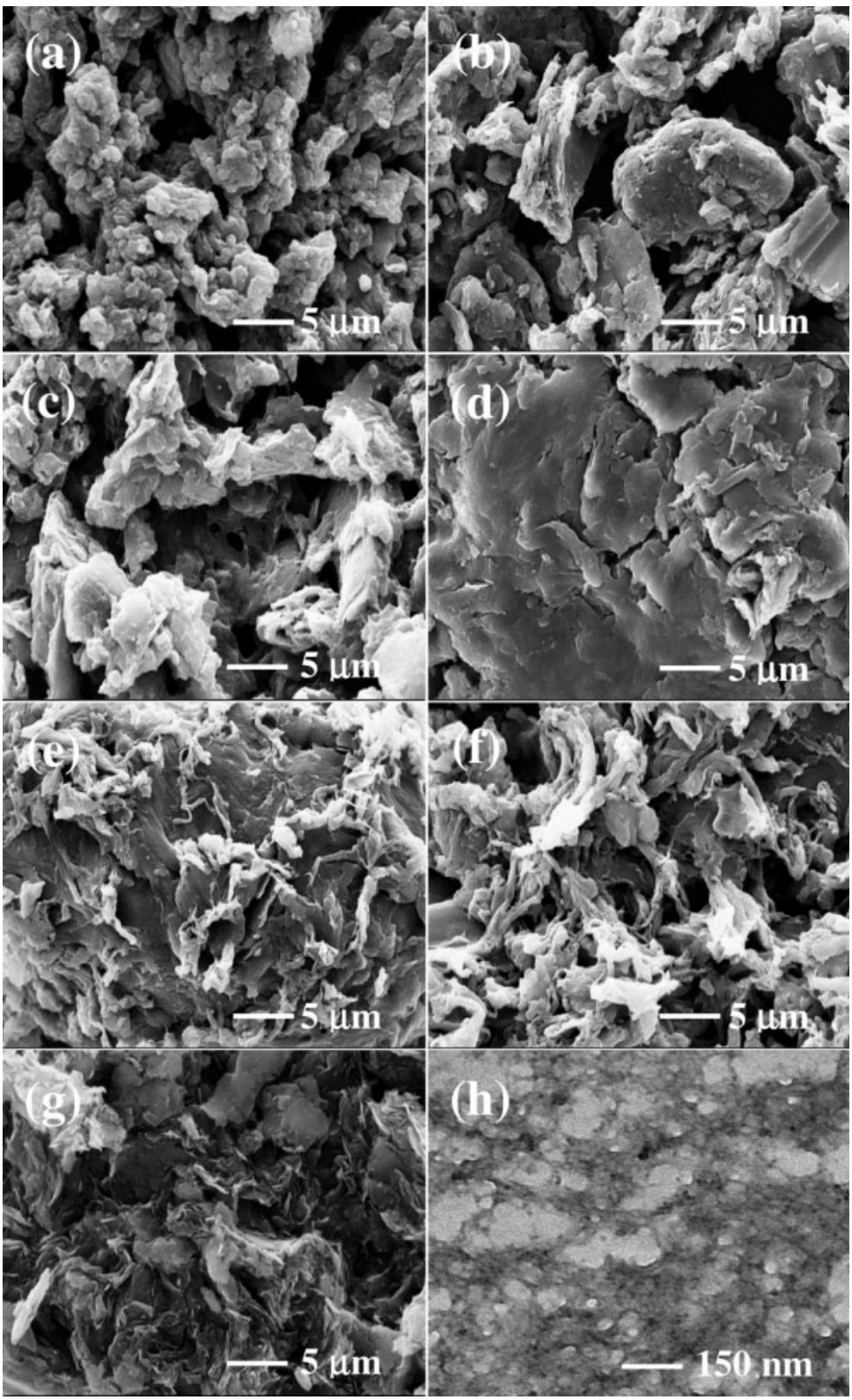

Figure 4 SEM micrographs of polyaniline and polyaniline–graphite composites (a) GDBS0, (b) GDBS10, (c) GDBS30, (d) GDBS50, (e) GDBS70, (f) GDBS90, (g) GDBS100, and (h) TEM image of GDBS50.

temperature conductivity (σ) of the pellet can be calculated as:

$$\sigma = L/RA, \tag{2}$$

where L is the length of the pellet, R is resistance, and A is cross-sectional area of the pellet. The conductivity values are reported in Table I and represent the average of three samples. The conductivity

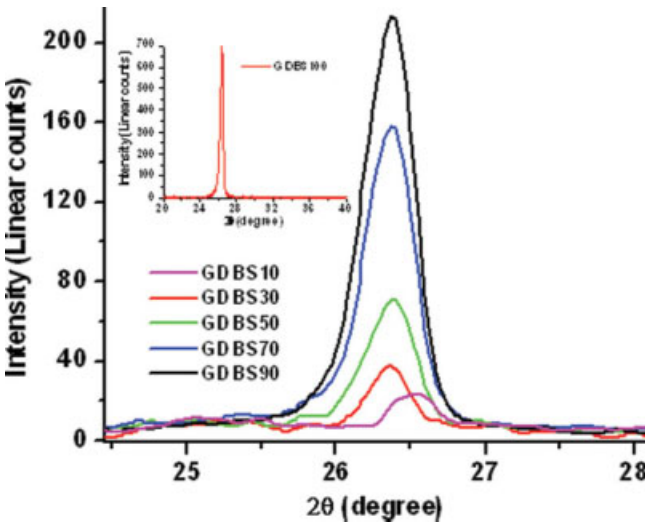

Figure 5 XRD patterns of graphite and polyaniline graphite composites. [Color figure can be viewed in the online issue, which is available at www.intersience.wiley.com.]

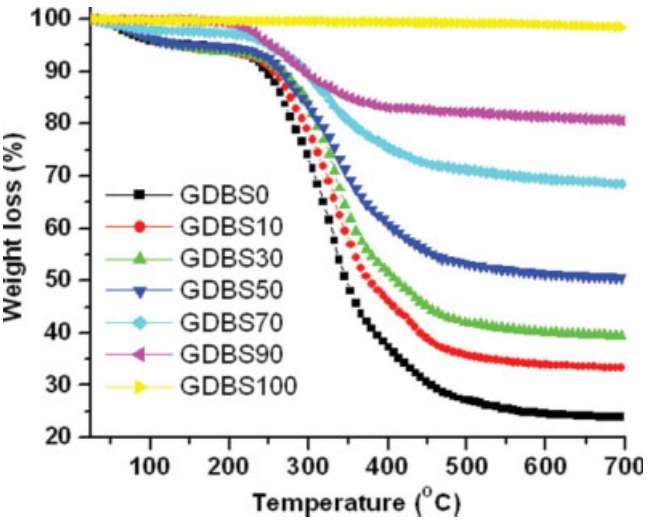

Figure 7 TG traces of graphite, polyaniline, and polyaniline–graphite composites. [Color figure can be viewed in the online issue, which is available at www.intersience.wiley.com.]

continuously increases with the graphite proportion. This is due to the highly conducting nature of graphite, which acts as a conducting bridge between the crystalline (metallic) aggregates of polyaniline. The number of interconnecting conducting networks increases with increasing graphite amount, leading to enhancement in conductivity. The conductivity (Fig. 6) initially increases at a slower rate, then attains a plateau and finally increases exponentially. This nonlinear conductivity rise suggests the systematic changes in specific interactions between graphite and polyaniline. This may be due to the changeover in matrix from polyaniline (at low graphite content) to graphite (at higher graphite amount).

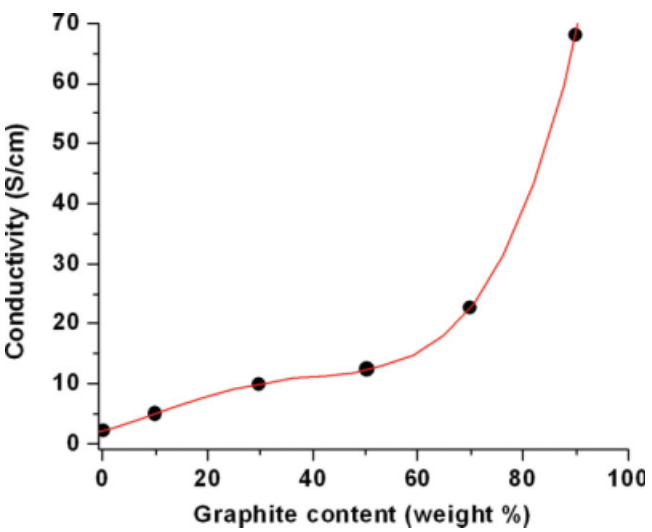

Figure 6 Effect of graphite content on the electrical conductivity of polyaniline–graphite composites. [Color figure can be viewed in the online issue, which is available at www.intersience.wiley.com.]

Thermogravimetric analysis

Figure 7 shows the thermogravimetric traces (TG) of pure graphite, polyaniline, and composites. The materials were heated from 25 to 700°C under a constant heating rate of 10°C/min in the inert atmosphere of nitrogen gas. These plots show that weight loss occurs in several systematic steps; each corresponds to the loss of particular species. The pure graphite (GDBS100) has excellent thermal stability up to 700°C, and weight loss was only 1.5%. In composites, the first loss at 120°C is attributed to the loss of adsorbed water molecules. As the graphite content increases, water content decreases due to the lower polyaniline content, which is the main hygroscopic species. The weight loss in the second step, i.e., ~ 230°C, involves the loss of $-SO_3H$ functional groups of dopant, chemisorbed water, as well as onset of degradation of polymeric backbone. The increasing graphite content has a little influence over initial decomposition temperature (IDT), which increases from 230°C (GDBS0) to 238°C (GDBS30) and decreases afterward. The third weight loss step between 250 and 550°C can be ascribed to the complete degradation of dopant as well as polymeric backbone. The composites show little weight loss between 550 and 700 °C, and the char residues remaining in this region are mainly thermally stable inert materials such as minerals and metallic impurities, graphite powder, and the carbonized polymeric and dopant fragments. Since the amount of residue increases with the increasing graphite fraction, it could be used to determine the amount of actually

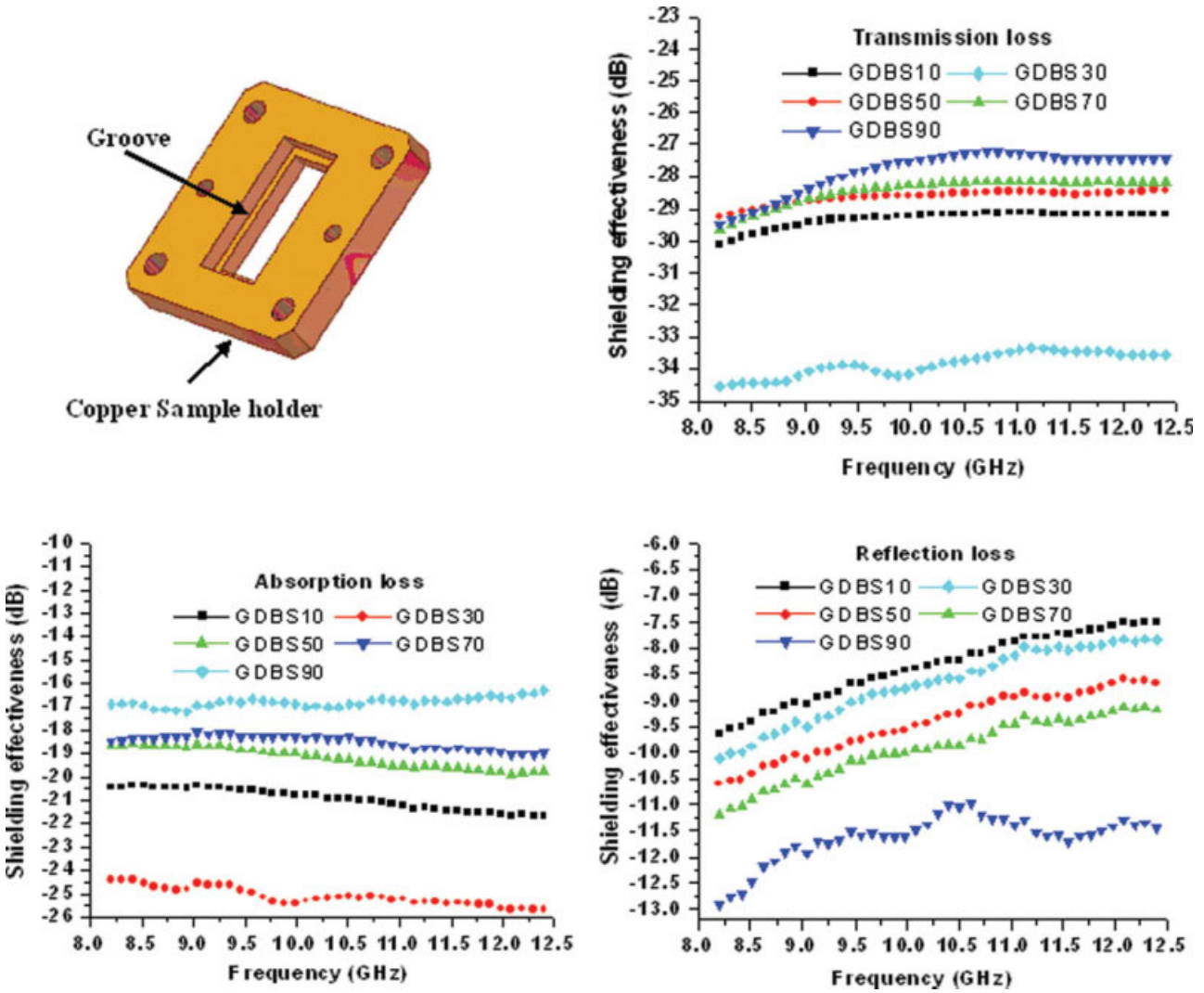

Figure 8 EMI shielding effectiveness of polyaniline graphite composites. [Color figure can be viewed in the online issue, which is available at www.intersience.wiley.com.]

incorporated graphite content. However, such estimation is based on the assumption that except from the graphite phase the percentage of all other inerts remain same in all composites and the graphite did not lose any weight at 550–700°C. Therefore, the graphite contents actually incorporated into the system were determined (reported in Table I) by taking the residue percentage of the pure doped polyaniline and subtracting it from the total residue of the respective composites. The results indicate that actually incorporated graphite content is much smaller than the corresponding weight ratio of aniline : graphite taken in the initial reaction mixture. This may be attributed to the weak noncovalent forces between polyaniline and graphite. The TGA data simply clarify that these composites have good thermal stability, even in vicinity of 230°C, which envisages them as a good candidate for melt blending with conventional thermoplastics such as PE, PP, and PS, etc.

Shielding effectiveness

EMI shielding is defined as the attenuation of the propagating electromagnetic waves produced by the shielding material. EMI SE can be expressed as[40–43]:

$$\text{EMI SE} = 10\log P_I/P_T = 20\log|E_I/E_T|(dB), \quad (3)$$

where $P_I(E_I)$ and $P_T(E_T)$ are the power (electric field) of incident and transmitted EM waves, respectively. For a single layer of shielding material, the EMI SE obtained from eq. (3) is described as the sum of the contribution due to reflection (SE_R), absorption (SE_A), and multiple reflections (SE_M) as the following[44,45]:

$$\text{SE} = \text{SE}_\text{R} + \text{SE}_\text{A} + \text{SE}_\text{M}\ dB \quad (4)$$

$$\text{SE}_\text{R} = 20\log|(1+n^2)/4n|dB \quad (5)$$

$$\text{SE}_\text{A} = 20\text{Im(k)d}\ \log e\ dB \quad (6)$$

$$SE_M = 20 \log |1 - (1 - n)^2/(1 + n)^2 \exp(2ikd)| \; dB \quad (7)$$

Here, n is the index of refraction of shielding material and Im (k) is the imaginary part of wave vector in the shielding material.

The S_{11} (or S_{22}) and S_{12} (or S_{21}) are the S parameters of the two-port network system and represent the reflection and transmission coefficients, respectively. The transmittance (T), reflectance (R), and absorbance (A) through the shielding material can be described as:

$$T = |E_T/E_I|^2 = |S_{12}|^2 (= |S_{12}|^2) \quad (8)$$

$$R = |E_R/E_I|^2 = |S_{11}|^2 (= |S_{22}|^2) \quad (9)$$

$$A = 1 - R - T \quad (10)$$

If the effect of multiple reflection between both interfaces of the material is negligible, the relative intensity of the effectively incident EM wave inside the materials after reflection is based on the quantity as $(1 - R)$. Therefore, the effective absorbance (A_{eff}) can be described as $A_{eff} = (1 - R - T)/(1 - R)$ with respect to the power of the effectively incident EM wave inside the shielding material. It is convenient that reflectance and effective absorbance are expressed as the form of $10/\log (1 - R)$ and $10/\log (1 - A_{eff})$ in decibels (dB), respectively, which provide the SE_R and SE_A as follows:

$$SE_R = 10 \log(1 - R) \; dB \quad (11)$$

$$SE_A = 10 \log(1 - A_{eff}) = 10 \log[T/(1 - R)] \; dB \quad (12)$$

In the case of non-negligible SE_M, however, the earlier relations are no longer valid, and further analysis of the S parameters is required.

The average value of shielding effectiveness (SE) of the composites [Fig. 8(b–d)] has been measured in the X band (8.2–12.4 GHz) by placing the sample pellets inside the sample holder [Fig. 8(a)] having a rectangular groove to hold the specimens. Despite an increase in graphite proportion, SE (Table I) increases only up to 30% graphite content and decreases afterwards. This indicates that some other loss mechanism apart from reflection (function of conductivity) plays a crucial role. To explore this behavior, we resolved the total shielding effectiveness into two components, i.e., absorption and reflection loss [Fig. 8(c,d)]. The results revealed that as expected, reflection loss increases with increasing graphite content. However, the absorption loss initially increases with graphite content up to GDBS-30 and then falls dramatically with further increase in graphite content. We attribute such an effect to increased interfacial interactions at low graphite content. However, at higher graphite percentages, such interactions decrease due to matrix changeover and phase segregation. Probably porosity of the composites also plays a significant role. Therefore, for achieving the best shielding properties, optimization of graphite amount is necessary. The acceptable values of absorption-dominated SE indicate that these materials could be utilized effectively for the shielding purposes in the X-band (8.2–12.4 GHz).

CONCLUSIONS

Highly conducting composites of polyaniline and graphite were prepared by in situ emulsion polymerization technique. Higher electronic conductivity and faster charge transport makes them potential candidates as an electrode material for battery applications. Morphological details revealed the presence of a layered structure in pure graphite and highly agglomerated globular particles in composites. UV–visible spectra showed systematic shifting of the characteristic peaks, indicating significant interactions between polyaniline and graphite. FTIR and XRD confirmed the presence of polyaniline in the composites. The electrical conductivity initially increased at a slower rate, then attained a plateau and finally increased exponentially. This suggests the systematic changes in interactions between graphite and polyaniline. Thermal data suggested that composites have good stability even in the vicinity of 230°C and thus could be used for melt blending with thermoplastics. The EMI shielding initially increased with graphite content up to GDBS-30 and then fell dramatically with further incorporation of graphite. Such effect may be ascribed to increased interfacial interactions at low graphite content. However, at higher graphite percentages, such interactions decreased due to matrix changeover and phase segregation. Therefore, for achieving the best shielding properties, optimization of graphite amount is necessary. The acceptable values of SE indicate that these materials could be utilized effectively for shielding purposes in the X-band. Our further studies will be concentrated on the melt blending of these composites with thermoplastics such as PE, PP, and PS.

The authors thank Director NPL for his keen interest in the work. The authors are also thankful to Dr. S.K. Halder of NPL for recording XRD patterns and Mr. Mukesh Khanna of IIT Delhi for TEM images.

References

1. Li, S.; Zhang, G.; Jing, G.; Kan, J. Synth Met 2008, 158, 242.
2. Canobre, S. C.; Davoglio, R. A.; Biaggio, S. R.; Rocha-Filho, R. C.; Bocchi, N. J Power Sources 2006, 154, 281.

3. Scorsone, E.; Christie, S.; Persaud, K. C.; Kvasnik, F. Sens Actuators B 2004, 97, 174.
4. Kilmartin, P. A.; Martinez, A.; Bartlett, P. N. Curr Appl Phys 2008, 8, 320.
5. Aussawasathien, D.; Dong, J. H.; Dai, L. Synth Met 2005, 154, 37.
6. Dhawan, S. K.; Trivedi, D. C. Synth Met 1993, 60, 67.
7. Qgurtsov, N. A.; Pud, A. A.; Kamarchik, P.; Shapoval, G. S. Synth Met 2004, 143, 43.
8. Jeyaprabha, C.; Sathiyanarayanan, S.; Venkatachari, G. J Appl Polym Sci 2006, 101, 2144.
9. Makeiff, D. A.; Huber, T. Synth Met 2006, 156, 497.
10. Dhawan, S. K.; Singh, N.; Rodrigues, D. J Sci Technol Adv Mater 2003, 4, 105.
11. Phang, S. W.; Tetsuo, H.; Abdullah, M. H.; Kuramoto, N. Mater Chem Phys 2007, 104, 327.
12. Barnes, A.; Despotakis, A.; Wright, P. V.; Wong, T. C. P.; Chambers, B.; Anderson, A. P. Electron Lett 1996, 32, 358.
13. Wycisk, R.; Pozniak, R.; Pasternak, A. J Electrostat 2002, 56, 55.
14. Soto-Oviedo, M. A.; Araújo, O. A.; Faez, R.; Rezende, M. C.; De Paoli, M. A. Synth Met 2006, 156, 1249.
15. Bloom, P. W. M.; Vissenberg, M. C. J. M.; Hulberts, J. N.; Martens, H. C. F.; Schoo, H. F. M. Appl Phys Lett 2000, 77, 2057.
16. Burroughes, J. H.; Bradley, D. D. C.; Brown, A. R.; Marks, R. N.; Mackay, K.; Friend, R. H.; Burns, P. L.; Holmes, A. B. Nature 1990, 347, 539.
17. Guatafson, G.; Cao, Y.; Treacy, G. M.; Klavetter, F.; Colaneri, N.; Heeger, A. J. Nature 1992, 357, 477.
18. Jou, J. H.; Hsu, M. F.; Wang, W. B.; Liu, C. P.; Wong, Z. C.; Shyue, J. J.; Chiang, C. C. Org Electron 2008, 9, 291.
19. Jain, S. C.; Aernout, T.; Kapoor, A. K.; Kumar, V.; Geens, W.; Poortmans, J.; Mertens, R. Synth Met 2005, 148, 245.
20. Yu, G.; Zhang, C.; Heeger, A. J. Appl Phys Lett 1994, 64, 1540.
21. Drelinkiewicz, A.; Hasik, M.; Kloc, M. J Catal 1999, 186, 123.
22. Rimbu, G. A.; Jackson, C. L.; Scott, K. J Optoelectron Adv Mater 2006, 8, 611.
23. Stafström, S.; Brédas, J. L.; Epstein, A. J.; Woo, H. S.; Tanner, D. B.; Huang, W. S.; MacDiarmid, A. G. Phys Rev Lett 1987, 59, 1464.
24. Dao, L. H.; Leclerc, M.; Guay, J.; Chevalier, J. W. Synth Met 1989, 29, 377.
25. Leclerc, M. J Electroanal Chem 1990, 296, 93.
26. Mattosso, L. H. C.; Faria, R. M.; Bulhoes, L. O. S.; MacDiarmid, A. G.; Epstein, A. J. J Polym Sci Part A: Polym Chem 1994, 32, 2147.
27. Umare, S. S.; Borkar, A. D.; Gupta, M. C. Bull Mater Sci 2002, 25, 235.
28. Savitha, P.; Rao, P. S.; Sathyanarayana, D. N. Polym Int 2005, 54, 1243.
29. Cao, Y.; Smith, P.; Heeger, A. J. Synth Met 1992, 48, 91.
30. Heeger, A. J. TRIP 1995, 3, 39.
31. Tchmutin, I. A.; Ponomarenko, A. T.; Krinichnaya, E. P.; Kozub, G. I.; Efimov, O. N. Carbon 2003, 41, 1391.
32. Du, X. S.; Xiao, M.; Meng, Y. Z. Eur Polym J 2004, 40, 1489.
33. Luo, K.; Guo, X.; Shi, N.; Sun, C. Synth Met 2005, 151, 293.
34. Saini, P.; Choudhary, V.; Dhawan, S. K. Ind J Eng Mater Sci 2007, 14, 436.
35. Saini, P.; Choudhary, V.; Singh, B. P.; Mathur, R. B.; Dhawan, S. K. Mat Chem Phys 2009, 113, 919.
36. Saini, P.; Jalan, R.; Dhawan, S. K. J Appl Polym Sci 2008, 108, 1437.
37. Philip, B.; Xie, J.; Abraham, J. K.; Vardan, V. K. Polym Bull 2005, 53, 127.
38. Bourdo, S. E.; Viswanathan, T. Carbon 2005, 43, 2983.
39. Howe, J. Y.; Rawn, C. J.; Jones, L. E.; Ow, H. Powder Diffraction J 2003, 18, 150.
40. Lee, C. Y.; Song, H. G.; Jang, J. S.; Oh, E. J.; Epstein, A. J.; Joo, J. Synth Met 1999, 102, 1346.
41. Hong, Y. K.; Lee, C. Y.; Jeong, C. K.; Lee, D. E.; Kim, K.; Joo, J. Rev Sci Instrum 2003, 74, 1098.
42. Wang, Y.; Jing, X. Polym Adv Technol 2005, 16, 344.
43. Singh, K.; Ohlan, A.; Saini, P.; Dhawan, S. K. Polym Adv Technol 2008, 19, 229.
44. Colaneri, N. F.; Shackeltte, L. W. IEEE Trans Instrum Meas 1992, 41, 291.
45. Joo, J.; Epstein, A. J. Appl Phys Lett 1994, 65, 2278.